Thermal Conductivity of Normal and Superconducting Indium-Lead Alloys*

Ronald E. Giedd† and C. A. Reynolds
Physics Department and Institute of Materials Science, University of Connecticut, Storrs, Connecticut 06268
(Received 17 June 1970)

Twelve InPb alloy samples with 3.00–8.00 at.% Pb concentrations were studied. These were divided into two sets, each consisting of six samples, one set with their c axis oriented approximately at 81°, and the other at approximately 14°, with respect to the sample axis. The electrical resistivities ρ at 4.2, 77, and 273 °K were measured, yielding the electrical anisotropies $a(4.2)$, $a(77)$, and $a(273)$, where $a=\rho_\perp/\rho_\parallel$. These verified the earlier findings of Carriker. For the pure In, $a(77)=0.986\pm0.003$ and $a(273)=1.041\pm0.003$, showing the same shift in maximum resistivity from the c to the a direction as the temperature is increased from 77 to 273 °K. Also, the anomalies at 3.50 and 7.00 at.% Pb were again seen. The thermal conductivities were measured for all samples in both the normal and the superconducting state. In the normal thermal conductivities at 3 °K, the anisotropy was $a=1.077$ for the 3.00-at.%-Pb samples, and $a=1.054$ for the 8.00-at.%-Pb samples where $a=K_\parallel/K_\perp$. The anomalies at 3.50 and 7.00 at.% Pb were evident. A temperature minimum existed in the superconducting thermal conductivity for all samples and was a linear function of Pb concentration for both sets, slowly increasing with increasing concentration from a temperature of 1.66–2.1 °K. The normal lattice thermal conductivity was never more than 10% of the total thermal conductivity; it is accounted for by phonon-electron interaction scattering, mass-defect scattering, and scattering due to distortion of the lattice around the mass defect; and it was anisotropic. It was found that adding the squares of the strengths of the scattering mechanisms gave a better fit than adding the mean square-root values and then squaring, since the phases of the scattering mechanisms were not known. The ratio K_{gs}/K_{gn} was plotted as a function of the reduced temperature and compared with the Klemens-Tewordt theoretical expression.

I. INTRODUCTION

This paper describes an experimental investigation of the effects of mass defects on the thermal conductivity of normal and superconducting In-Pb alloys. In was selected as a host for the heavier Pb atoms as a continuation of the general experimental study of the electrical and superconducting properties of InPb alloys by this laboratory.

Recent investigation[1] of the electrical resistivity of the InPb alloys in the 0-at.%–9.00-at.%-Pb range revealed the existence of an anisotropy in $\rho_{4.2}$, ρ_{77}, and ρ_{273}, where ρ_T is the resistivity at the temperature T. This anisotropy was explained using the method by Klemens *et al.*[2] and Carriker *et al.*[1] that evaluated the sections of the Fermi surface that does not contribute to the electrical conductivity because of its contact with Brillouin-zone boundaries of nonvanishing structure factor.

Also this early investigation found anomalies in various electrical quantities at 3.50 at.% Pb and in the superconducting transition temperature T_c at 7.00 at.% Pb.[3] These were consistent with the results of other investigations on the lattice anisotropy,[4] specific heat,[5] and T_c, and were explained using the Fermi-surface–Brillouin-zone interaction model of Goodenough.[6] The anomalies were explained by assuming that the Fermi surface just intersected the (200)-zone boundary and overlapped the (002)-zone boundary in pure In. As the Pb doping was increased, the added electrons forced the (002)-zone boundary in and the (200)-zone boundary out until, at 3.50 at.% Pb, an adjustment takes place, resulting in an increase in the number of electrons available for conduction in the a direction Further doping causes the Fermi surface to pop through the (200)-zone boundary at 7.00 at.% Pb, again increasing the number of electrons available for conduction in the a direction and causing the second anomaly.

The thermal conductivity of the normal metal is

$$K_n=K_{en}+K_{gn}, \tag{1}$$

where K_{en} is the electronic thermal conductivity described by the Wiedemann-Franz Law and K_{gn} is the lattice thermal conductivity.

The existence of solute atoms in the In raises the possibility of three different scattering processes for the phonons: (a) the usual phononelectron interaction, (b) scattering due to the difference in mass ΔM between the In atoms and Pb atoms, and (c) scattering caused by the distortion of the lattice around the Pb atoms. To a very rough approximation, the thermal resistivities $W=1/K$ of these processes could be added together so that

$$W_{gn}=W_{pe}+W_{\Delta M}+W_{dis}, \tag{2}$$

where $W_{gn}=1/K_{gn}$, W_{pe} is the resistivity due to phonon-electron interaction, $W_{\Delta M}$ is the resistivity due

to mass difference, and W_{dis} is the resistivity due to lattice distortion. However, this is inexact whenever there is a difference in phonon frequency dependence for the various interaction processes. The exact equation is found by adding the reciprocal of the phonon mean free paths for the processes. Thus

$$1/l(\omega) = \sum_i 1/l_i(\omega), \tag{3}$$

where $l(\omega)$ is the resulting mean free path for a phonon with frequency ω, and $l_i(\omega)$ is the mean free path due to the ith scattering process. For combined phonon scattering by electrons and by point defects the lattice thermal conductivity is

$$K_g = BT^2\, I(\alpha)/7.21, \tag{4}$$

where

$$I(a) = \int_i^\infty \frac{x^3\, e^x\, dx}{(e^x-1)^2(1+a\,x^3)}\ , \tag{5}$$

$$a = \frac{12\pi^2 a^3}{7.21\, v^2\, \hbar}\ S^2 BcT^3, \tag{6}$$

and v is the velocity of sound, a is the lattice constant, c is the concentration of point defects, and $B = K_{ng}/T^2$ for the purest sample. The scattering amplitude is $S^2 = S_1^2 + S_2^2$, where S_1 is due to the mass defect, i.e.,

$$S_1^2 = \tfrac{1}{12}\,(\Delta M/M)^2. \tag{7}$$

M is the average atomic mass and S_2 is due to distortion, i.e.,

$$S_2^2 = 3\gamma^2\,(\Delta R/R)^2, \tag{8}$$

where γ is the Grüneisen constant, assumed to be 2 in this experiment, and $\Delta R/R$ is the fractional radial distortion of the lattice.[7]

The superconducting thermal conductivity is

$$K_s = K_{es} + K_{gs}, \tag{9}$$

where K_{es} is the electronic thermal conductivity and K_{gs} is the phonon thermal conductivity in the superconducting state.

Since all measurements for this investigation were made on In containing at least 3.00 at.% Pb, the BRT theory[8] was used to calculate K_{es}. When impurity scattering dominates, the ratio of the superconducting to the normal electronic thermal conductivity is

$$\frac{K_{es}}{K_{es}} = \frac{2F_1(-y) + 2y\ln(1+e^{-y}) + y^2/(1+e^y)}{2F_1(0)}, \tag{10}$$

where $y = \epsilon_0(T)/k_B$, $2\epsilon_0(T)$ is the superconducting energy gap, and $F_n(-y)$ are Fermi-Dirac integrals evaluated by Rhodes.[9] With this equation the superconducting lattice conductivity can be separated out and the ratio K_{gs}/K_{gn} can be computed.

Klemens and Tewordt[10] have a theoretical expression for K_{gs}/K_{gn} in the presence of point defects described by the same α coefficient [see Eqs. (5) and (6)] for both the superconducting lattice thermal conductivity and the normal lattice thermal conductivity. This expression is

$$\frac{K_{gs}}{K_{gn}} = \frac{\int_0^\infty x^3 e^x\, dx (e^x-1)^2\,[g(x)+\alpha\, x^3]^{-1}}{\int_0^\infty x^3 e^x\, dx (e^x-1)^2\,(1+\alpha x^3)^{-1}}\ . \tag{11}$$

However, the α used in their original theoretical equation contained just the S_1^2 term and ignored the S_2^2 term – an approximation that will be shown to be in disagreement with the experimental results.

II. EXPERIMENTAL DETAILS

The low-temperature apparatus and thermal-conductivity data reduction procedure have been described in various other papers.[11,12] The method employed was a steady-state heat-flow method, holding one end of the sample at the bath temperature and heating the other end to produce a temperature gradient along the sample. The conductivity measurements were taken approximately every 0.1 °K in the 1.3–4.2 °K temperature interval.

Germanium-resistance thermometers were used to measure all the temperatures. These thermometers were calibrated at approximately 0.100 °K intervals going from 4.2 to 1.06 °K by placing them directly in the liquid-helium bath and then calibrating against the 1958 Helium Vapor Pressure Tables. A heater was placed at the bottom of the helium Dewar in order to destroy any stratification of the liquid for all calibration measurements above the λ point.

These calibration points were fitted by the method of least squares to an equation of the form[12,13]

$$T^{-1} = A + B\ln R + C/\ln R + D(\ln R)^2 + E/(\ln R)^2. \tag{12}$$

These fits, along with the deviation curves, were used to convert the resistances to the corresponding temperatures.

Twelve samples were used, all single crystals grown by the Bridgemann technique in glass crucibles constructed from 2-mm-i.d. precision glass tubing. All samples were approximately 8 cm long and with a diameter of 2 mm. They were oriented using an optical goniometer[14] and were chosen so that six were oriented with the c axis approximately 14° from the sample axis (hereafter called the parallel samples) and six were oriented with the c axis approximately 81° from the sample axis (hereafter called the perpendicular samples), with the exception of a 7.00-at.% sample that was oriented at 60° with respect to the c axis. Each set contained samples with 3.00-, 3.50-, 4.00-, 6.00-, 7.00-, 8.00-at.%-Pb concentration.

Electrical resistivity measurements were made at 4.2, 77, and 273 °K on all samples using a microvolt potentiometer (Honeywell model No. 2783)

for the potential measurements and a Honeywell digital voltmeter reading the voltage drop on a 100-Ω Leeds and Northrup standard resistor for the current measurement.

Three thermal conductivity runs were performed on each sample. These were (a) a run on the superconducting metal, then (b) a run at a temperature well below the superconducting transition temperature during which the temperature gradient and sample temperature were held constant and an applied magnetic field was increased. This determined the critical fields for the alloys, and furthermore would have revealed any magnetoresistive effects if they existed. None were seen. (c) Finally, the magnet was set at a field well above the critical field of the sample, and a thermal-conductivity run was made on the normal alloy.

III. RESULTS AND DISCUSSION

A. Normal and Superconducting Thermal Conductivity

The results of all the data runs are shown in Figs. 1(a) and 1(b). The normal thermal conductivities all exhibit approximately 9% lattice thermal conductivity. In general, they are linear functions of temperature.

An anisotropy is readily apparent in both the normal and superconducting thermal conductivities; these are shown in Fig. 2 along with the anisotropy in the electrical resistivity. Anomalous variations of anisotropy with concentration caused by interaction between the Fermi surface and Brillouin zones are in evidence, particularly in the normal-thermal-conductivity anisotropy. This, of course,

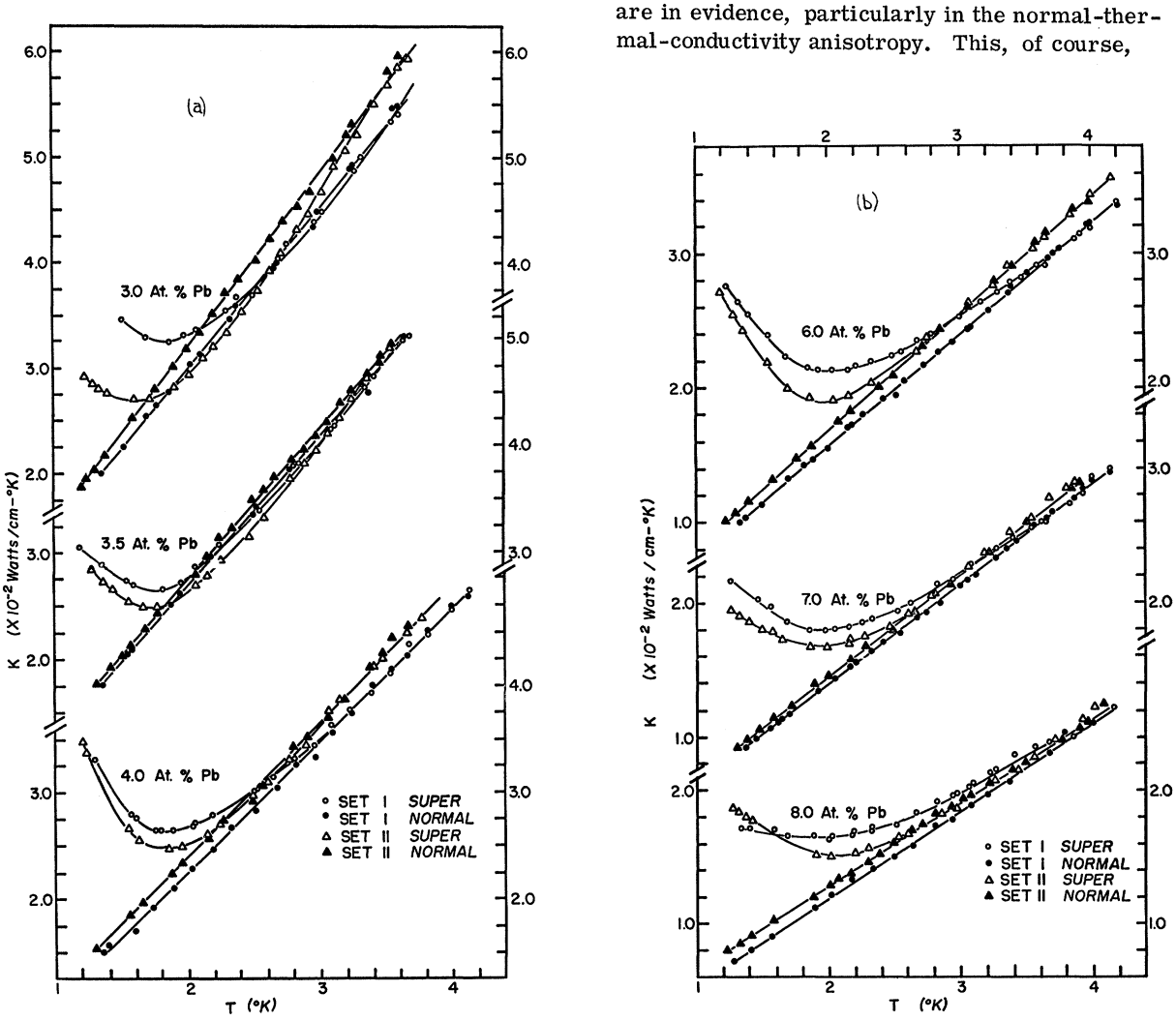

FIG. 1. (a) Total thermal conductivity for the most dilute samples in both their superconducting and normal state configurations versus temperature; (b) total thermal conductivity for samples containing the higher Pb concentrations in both their superconducting and normal state configurations versus temperature. Set-I samples are the perpendicular samples and set-II samples are the parallel samples. The superconducting runs are denoted by O and Δ and the normal runs by • and ▲.

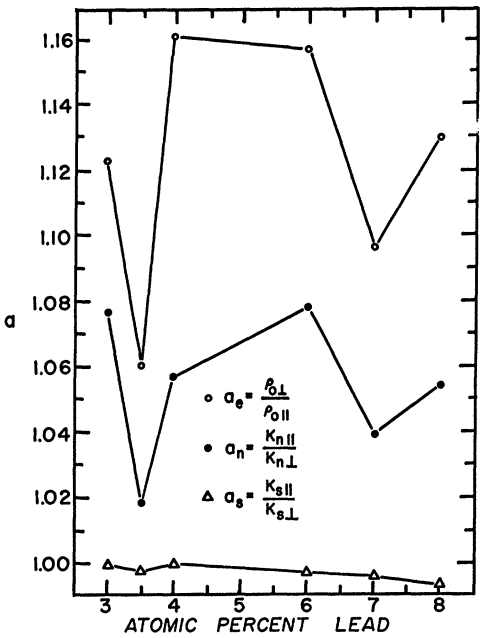

Fig. 2. The anisotropy in the electrical resistivity ○, in the normal state thermal conductivity ●, and in the superconducting thermal conductivity △ versus the Pb concentration.

strongly indicates that the source of this anisotropy lies in the electric component as is expected since this is the primary conductivity mechanism. However, the anisotropy in the normal thermal conductivity $a_n = K_{n\parallel}/K_{n\perp}$ is smaller than the electrical resistivity anisotropy $a_e = \rho_\perp/\rho_\parallel$. As shall be shown in Sec. III B, the lattice thermal conductivity is also anisotropic, but in the opposite sense. Thus, since

$$a_n = K_{n\parallel}/K_{n\perp} = (K_{en\parallel} + K_{gn\parallel}/K_{en\perp} + K_{gn\perp}),$$

but

$$K_{gn\perp} < K_{gn\parallel},$$

the resulting anisotropy is less than that predicted by the electrical resistivities. Further proof of this can be seen in the anisotropy in the superconducting thermal conductivity $a_s = K_{s\parallel}/K_{s\perp}$, where the anomlies are severaly depressed for a temperature well below the transition temperature of the alloy. At these temperatures the normal electron density has fallen off to such an extent that the lattice conductivity is beginning to predominate. Hence, a_s is beginning to assume the shape of the anisotropy curve for the lattice thermal conductivity.

The superconducting curve in the more dilute alloys exhibit an initial decrease below the normal curve because the electronic thermal conductivity is being decreased by the formation of superconducting electron pairs. This reduces the thermal conductivity of the sample until the normal electrons are so decreased in number that phonon-electron interactions no longer limit the lattice conductivity. At this point, the increasing lattice thermal conductivity begins to be noticeable, and the thermal conductivity of the superconducting sample swings above the normal conductivity.

For the more impure samples, starting with the 4.00-at.% alloy, the point defects, which scatter electrons more strongly than phonons, have decreased the electronic contribution to such an extent that the increasing lattice term in the superconducting state starts to become predominant before the electronic reduction can be seen.

In all cases the superconducting conductivity curves show a conductivity minimum where the increase in the lattice term overcomes the decrease in the electronic thermal conductivity. Since point defects limit the electronic component more than the phonon component in the first place, it is reasonable to expect this minimum to become evident sooner as the point-defect concentration is increased. Evidence of this is seen in Fig. 3, where the temperatures of these thermal-conductivity minima are shown to have a linear dependence on the point-defect concentration.

B. Lattice Thermal Conductivity of Normal Alloys

The lattice conductivity can be separated out by

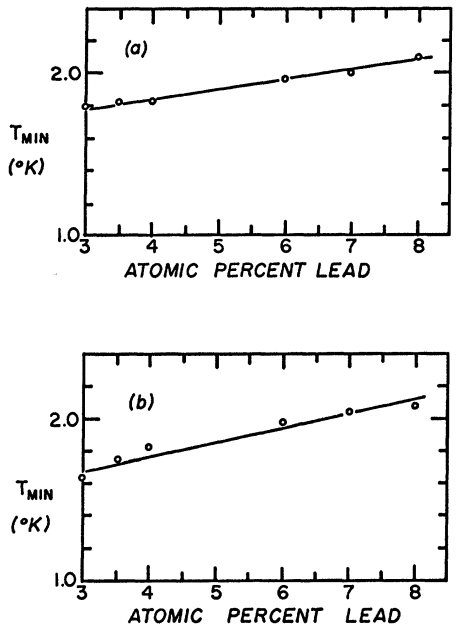

FIG. 3. (a) Temperature at which the superconducting thermal conductivity is a minimum for the perpendicular samples versus Pb concentration; (b) temperature at which the superconducting thermal conductivity is a minimum for the parallel samples versus Pb concentration.

subtracting the electronic component

$$K_{gn} = K_n - K_{en} ,$$

where K_{en} is the electronic component, calculated from the electrical resistivity by the Wiedemann-Franz law. All the normal lattice conductivities are shown in Fig. 4.

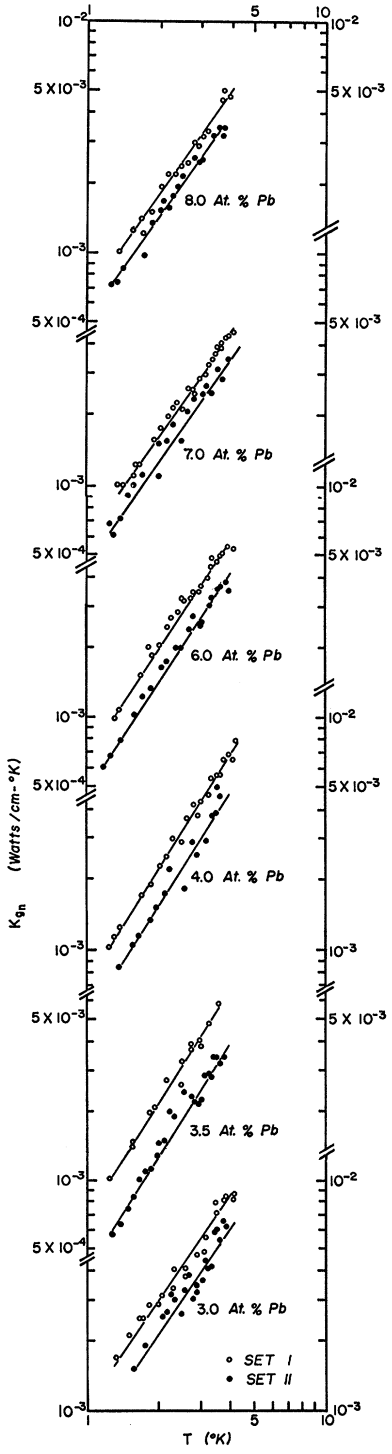

FIG. 4. Lattice thermal conductivity for all samples as a function of temperature on a log-log plot to show its temperature dependence. Set I, denoted by ○, are the perpendicular samples and set II, denoted by •, are the parallel samples.

As can be seen, all the K_{gn}'s are temperature dependent, following the equation $K_{gn} = bT^m$, where m is positive and greater than 1. The values of the slopes of all these curves (therefore the value of m) are shown in Fig. 5 as a function of the point-defect concentration. Two things are obvious from this figure: first, that there is no anisotropy in the value of m, and second, that m decreases linearly as the solute content increases. Thus, the scattering caused by point defects and lattice distortion becomes stronger as the Pb concentration increases.

Experimental values for α [see Eq. (6)] were obtained using Eqs. (4) and (5) and evaluating $I(\alpha)$ as a function of α with an IBM 360 computer. The second column of Table I lists the resulting experimental values of α along with a measure of the uncertainty in the numbers due to the scatter in the data.

The third columm is the theoretical values of α obtained from Eq. (6) and assuming the existence of only mass-defect scattering, thus letting $S^2 = S_1^2$. As can be seen, these computed values are only half as large as the experimental values; therefore, the lattice distortion term [Eq. (8)] was included in the compution of S^2.

The fractional radial distortion taken from the observed change in the lattice spacings[4] of InPb alloys in $\Delta R/R = 0.19$. This value, used in Eq. (8), raises the theoretical value above the experimental values listed. This may be because the distortion ratio $\Delta R/R$ calculated from the available data is too large. It can be seen that the discrepancy between the experimental and theoretical values for α in the dilute alloys is larger than in the more highly concentrated samples. The third column lists the resulting theoretical α values, accounting for distortion scattering.

These final theoretical α_{md} values were calculated assuming $S^2 = S_1^2 + S_2^2$. However, it is possible to calculate an S^2 from the relationship $S^2 = (S_1 + S_2)^2$, but S_1 and S_2 have an unknown phase relation that makes it difficult to sum them together in this way. If they are calculated using the square roots of Eqs. (7) and (8), the resulting S^2 gives a scattering strength α, much larger than that computed using $S^2 = S_1^2 + S_2^2$. This obviously means that S_1 and S_2 are not in phase with each other, and it is better to square them first to remove the phase relationship before adding them together to form S^2.

Some thought was given to including a correction in the distortion term for the electronic dilatation effect of the added electrons on the lattice. However, this accounts for only approximately 1% of the $\Delta R/R$ and is less than the uncertainty in the experimental value of α. It was, therefore, not included in the final theoretical value of α.

To summarize, it seems probable that the lattice conductivity of these InPb alloys is a result of a

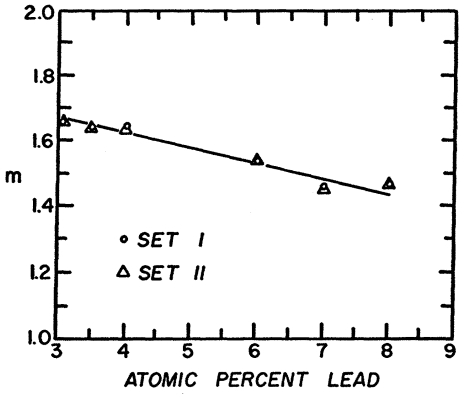

FIG. 5. Slope of the lines in Fig. 4 as a function of concentration. Here m is the power of T in the equation $K_{gn} = bT^m$, where b is some constant. Set I, denoted by O, is the set of perpendicular samples, and set II, denoted by Δ, is the set of parallel samples.

number of processes; first, phonon-electron scattering; second, mass-defect scattering; and third, in nearly equal strength, anharmonic scattering due to distortion of the lattice.

Figure 6 is a graph of the anisotropy in the lattice conductivity as a fucntion of the Pb content. It should be noticed that this phonon anisotropy ranges around 45%, as opposed to only about 6% for the space-lattice anisotropy and the electrical-resistivity anisotropy. It is somewhat gratifying to see that this curve has the same general shape as the lattice-anisotropy curve taken from the literature.[1] They both reach a maximum and decrease in value at both ends of the alloy range, although the maximum in the space-lattice anisotropy is at 7.0 at.% Pb, not 6.0 at.% Pb. This is not too disturbing, because the 7.00-at.% sample is oriented at 60° with

TABLE I. α versus point-defect concentration.

at.% Pb	α_{expt} ($\times 10^{-3}$)	α_m ($\times 10^{-3}$)	α_{md} ($\times 10^{-3}$)
Samples with c axis ⊥ to sample axis			
3.00	2.75±0.22	2.0	3.79
3.50	3.45±0.21	2.1	3.98
4.00	3.60±0.21	2.3	4.36
6.00	5.10±0.20	3.3	6.25
7.00	7.0 ±0.20	4.2	7.96
8.00	7.7 ±0.19	4.4	8.34
Samples with c axis ∥ to sample axis			
3.00	2.75±0.22	1.72	3.31
3.50	3.43±0.21	1.8	3.47
4.00	3.75±0.20	1.98	3.81
6.00	5.2 ±0.20	2.84	5.47
7.00	6.9 ±0.19	3.52	6.97
8.00	7.0 ±0.19	3.78	7.28

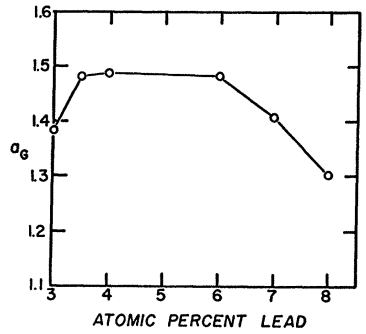

FIG. 6. Anisotropy in the lattice thermal conductivity versus Pb concentration.

respect ot the c axis, and is certainly not to be considered a perpendicular sample.

The lattice-thermal-conductivity anisotropy might also be related to the anisotropy in the velocity of sound in InPb alloys. However, there is little information on this in the literature, and it is difficult to tie the two together at this stage.

C. Ratio of Normal and Superconducting Lattice Thermal Conductivity

The ratio K_{gs}/K_{gn} is plotted as a function of the reduced temperature for each set of samples in Figs. 7 and 8. The curves in general fall off at each reduced temperature with increasing Pb content because mass-defect scattering becomes dominant in both states, as predicted by the Klemens-Tewordt theory.[10] The dotted lines are theoretical curves using Eq. (11) and their equation for α, assuming only the presence of mass-defect scattering. The values for α for these curves are calculated for alloys in the 6-at.%-Pb range using the Klemens-Tewordt expression for α. The discrepancies between the theoretical and experimental curves are probably caused by the absence of a distortion term in the theoretical expression. It is felt that the results show that the scattering processes leading to the expression for α are the same in both the normal and the superconducting states.

IV. SUMMARY

The observed values of the total normal-thermal-conductivity anisotropy were explained by accounting for the observed electrical-resistivity anisotropy noted in a previous paper,[1] and the anomalies were explained by investigating the Fermi-surface–Brillouin-zone interaction again, and shown also to originate in the electronic thermal-conductivity term in the total thermal conductivity.

The normal lattice thermal conductivity was found to be proportional to the temperature to some power, which decreased with increasing mass-defect concentration. This temperature dependence was

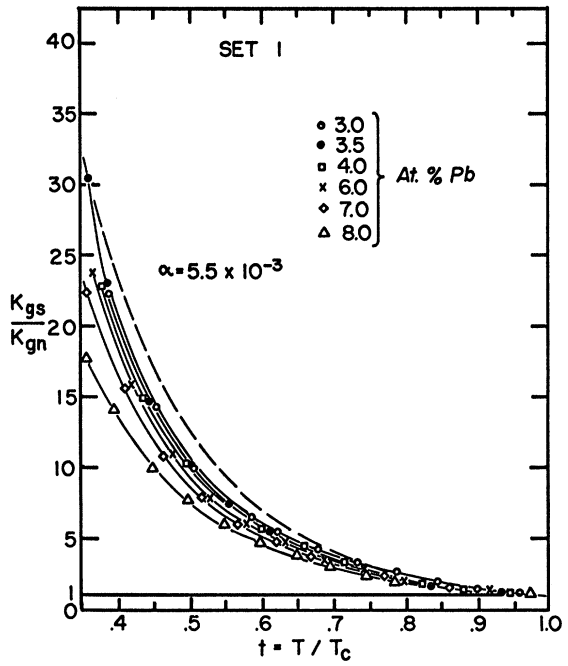

FIG. 7. Ratio of the lattice thermal conductivities as a function of reduced temperature for the perpendicular s samples. The 3.0-at.% sample is denoted by ○, the 3.50-at.% sample by ●, the 4.00-at.% sample by □, the 6.00-at.% sample by X, the 7.00-at.% sample by ◇, and the 8.00-at.% sample by Δ. The dashed curve is a theoretical result.

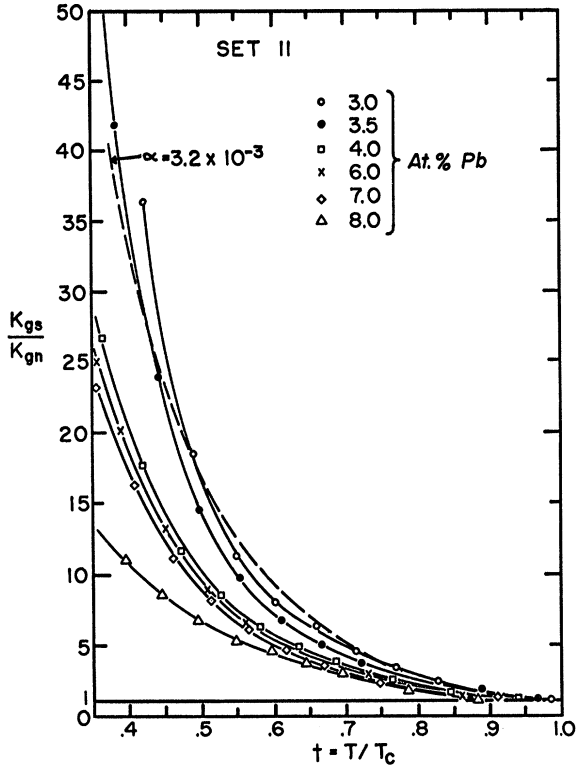

FIG. 8. Ratio of the lattice thermal conductivities as a function of reduced temperature for the parallel samples. The 3.0-at.% sample is denoted by ○, the 3.50-at.% sample by ●, the 4.00-at.% sample by □, the 6.00-at.% sample by x, the 7.00-at.% sample by ◇, and the 8.00-at.% sample by Δ. The dashed curve is a theoretical result.

shown to be a combination of three phonon-scattering processes: electron-phonon interactions, mass-defect scattering, and scattering by the anharmonic distortional field around the defect sites. Furthermore, it was shown that the scattering strenghts of the mass defects and their strain fields were approximately equal for most of the samples.

The agreement with the Klemens-Tewordt theoretical predictions showed that α for both the normal and the superconducting thermal conductivity is described by Eqs. (6)–(8).

Also, the investigation of the lattice thermal conductivity showed that the scattering amplitude S^2 is better described by $S^2 = S_1^2 + S_2^2$ than by $S^2 = (S_1 + S_2)^2$, since we have no knowledge of the relative phases of the different scattering processes.

ACKNOWLEDGMENTS

The authors are indebted to M. A. Mitchell for his invaluable aid in the various steps of this investigation, to Professor P. G. Klemens for his many comments and discussions, and to Hugh Taylor for technical assistance. The computational part of this work was carried out in the Computer Center at the University of Connecticut, which is supported in part by Grant No. GP-1819 of the National Science Foundation.

*Work supported by the U. S. Air Force Office of Scientific Reaserch Grant No. AF-AFOSR-474-67 and the Office of Naval Research under Contract No. NONR 2967(00).

†Present address: Stamford Branch of the University of Connecticut, Stamford, Conn.

[1]R. C. Carriker and C. A. Reynolds, Phys. Rev. (to be published).

[2]P. G. Klemens, C. Van Baarle, and F. W. Gorter, Physica 30, 1470 (1964).

[3]R. C. Carriker and C. A. Reynolds, Phys. Rev. (to be published).

[4]C. Tyzack and G. Raynor, Trans. Faraday Soc. 50, 675 (1954).

[5]S. Gygax, J. L. Olsen, and R. H. Kropschot, in *Low-Temperature Physics LT9*, edited by J. G. Daunt (Plenum, New York, 1965).

[6]J. B. Goodenough, Phys. Rev. 89, 282 (1953).

[7]J. E. Gueths, P. L. Garbarino, M. A. Mitchell, P. G. Klemens, and C. A. Reynolds, Phys. Rev. 178, 1009

(1969).
[8]J. Bardeen, L. N. Cooper, and J. R. Schrieffer, Phys. Rev. 108, 1175 (1957).
[9]P. Rhodes, Proc. Roy. Soc. (London) A204, 396 (1950).
[10]P. G. Klemens and L. Tewordt, Rev. Mod. Phys. 36, 118 (1964).
[11]J. E. Gueths, N. N. Clark, D. Markowitz, F. V. Burckbuchler, and C. A. Reynolds, Phys. Rev. 163, 364 (1967).
[12]P. L. Garbarino and C. A. Reynolds, Phys. Rev. (to be published).
[13]G. J. Pearson, C. W. Ulbrich, J. E. Gueths, M. A. Mitchell, and C. A. Reynolds, Phys. Rev. 154, 329 (1967).
[14]J. E. Gueths, F. V. Burckbuchler, and C. A. Reynolds, Rev. Sci. Instr. 40, 1344 (1969).

PHYSICAL REVIEW B VOLUME 2, NUMBER 9 1 NOVEMBER 1970

Current-Pulse Effect in the Intermediate State of Superconducting Lead Films*

R. P. Huebener
Argonne National Laboratory, Argonne, Illinois 60439
(Received 9 February 1970)

The enhancement of the resistive voltage in the intermediate state of superconducting lead films due to a high current pulse has been studied at 4.2 °K as a function of the width of the pulse τ, the magnetic field H, and the film thickness. The film thickness ranged between 1 and 7 μm. The resistive voltage increment after the current pulse, plotted versus τ, yields S-shaped curves which saturate at high values of τ. The half-time τ^* decreases strongly with increasing H. Assuming that the voltage increment is caused by the formation of a laminar flux structure perpendicular to the current during the pulse, the product of τ^* and the flux-flow velocity v_φ during the pulse can be expected to be of the order of the periodicity length of the laminar flux structure. Estimating v_φ at the pulse current from the flux-flow resistivity at small currents, the product $\tau^* \times v_\varphi$ increases with increasing film thickness and is in reasonable agreement with the value expected from Landau's model of the intermediate state. The current-pulse effect disappears below a film thickness between 1 and 2 μm. This can be understood from the experiments of Cody and Miller, which suggest that below a film thickness of about 1.5 μm lead films behave like type-II material.

INTRODUCTION

The electrical resistance in the intermediate state of type-I superconductors, in general, consists of two contributions: the Ohmic resistance within the normal regions and the flux-flow resistance due to the motion of the normal regions. The importance of flux-tube motion for the electrical resistance in the intermediate state has been demonstrated convincingly in recent experiments on the Ettingshausen[1,2] and Nernst effect,[3,4] and magnetic coupling,[5,6] and in the visual observation of the motion of the flux structure in the presence of an electrical current.[6,7] Further evidence for flux flow in type-I superconductors has been obtained from measurements of the noise voltage associated with a current.[8] The relative contribution of both terms to the electrical resistance depends on the arrangement of the flux structure in the intermediate state. As one approaches the critical field, the contribution from flux flow becomes less and less important. The arrangement of the flux structure in the intermediate state can be changed strongly by an electrical current. Passing a high current through the specimen results in the formation of a laminar flux structure in which the laminae are oriented predominantly perpendicular to the current direction.[6,9] The formation of this laminar structure leads to a hysteresis in the electrical resistance. Such a hysteresis has been reported first by Andrew[10] and has been studied in detail recently by Solomon.[6] In these experiments, the voltage was measured as a function of current while the current was raised from zero to a high value and then returned to zero. Recently, we have reported a current induced enhancement of the resistive voltage in the intermediate state of lead films using a somewhat different approach.[11] We have measured the voltage-current curves for relatively small currents before and after a *pulse of high current* had been passed through the specimen. A high-current pulse was found to cause an appreciable enhancement of the resistive voltage indicating a permanent rearrangement of the flux structure probably towards a laminar pattern perpendicular to the current.

A study of this current-pulse effect[11] as a function of the pulse width should indicate how the laminar pattern is gradually formed. From such measurements, knowing the flux-flow velocity during the current pulse, we can estimate the average distance each flux tube must travel to form the laminar pat-